Published in final edited form as:
Lab Chip. 2013 April 21; 13(8): 1571–1577. doi:10.1039/c3lc41253a.

Measuring Cell Mechanics By Optical Alignment Compression Cytometry

Kevin B. Roth[a], **Charles D. Eggleton**[b], **Keith B. Neeves**[a,c], and **David W. M. Marr**[a]

[a]Department of Chemical and Biological Engineering, Colorado School of Mines, Golden, CO, USA 80401

[b]Department of Mechanical Engineering, University of Maryland Baltimore County, Baltimore, MD, USA 21250

[c]Department of Pediatrics, University of Colorado, Denver, CO, USA 80045

Abstract

To address the need for a high throughput, non-destructive technique for measuring individual cell mechanical properties, we have developed optical alignment compression (OAC) cytometry. OAC combines hydrodynamic drag in an extensional flow microfluidic device with optical forces created with an inexpensive diode laser to induce measurable deformations between compressed cells. In this, a low-intensity linear optical trap aligns incoming cells with the flow stagnation point allowing hydrodynamic drag to induce deformation during cell-cell interaction. With this novel approach, we measure cell mechanical properties with a throughput that improves significantly on current non-destructive individual cell testing methods.

Introduction

Mechanical properties are one aspect of cell phenotype[1,2] that are a marker for diseases such as cancer,[1,3] diabetes,[4] sepsis,[5] malaria,[6] and sickle cell anemia;[7] for example, malaria infected red blood cells (RBCs) are more rigid than normal RBCs. To study this link between cell stiffness and phenotype, the mechanical properties of cells have been measured indirectly in solution as well as directly on individual cells. Ektacytometers,[8,9] cell filters,[10] and rheoscopes[8,11] measure properties of cell suspensions and yield average mechanical properties for cell populations; however, using these techniques it is difficult to identify small cell subpopulations such as circulating tumor cells. Micropipette aspiration,[6,12–14] atomic force microscopy,[3,15–17] magnetic tweezers[18,19] and single cell optical stretchers[20–22] measure the properties of individual cells but are low-throughput and consequently impractical for making measurements on cell populations.

To address the need for higher throughput measurements and identifying diseased sub-populations, deformation measurements on single cells have been reported in microfluidic-based devices. Measurement rates of 1–5 cell/s in optical stretching[21,22] and electroporation[23] coupled with flow have been achieved; however, these techniques can cause cell lysis by irreversibly damaging cell membranes. To avoid this, other approaches rely on collisions of cells with solid objects placed within a flow field to induce deformation where, for example, cells forced through a series of pillars yields a throughput of 1.7 cell/s.[24] A disadvantage of this approach is that it can be difficult to decouple cell-object

Corresponding Authors: David W. M. Marr, dmarr@mines.edu, Phone: 303-273-3008. Keith B. Neeves, kneeves@mines.edu, Phone: 303-273-3191. Department of Chemical and Biological Engineering, Colorado School of Mines, 1600 Illinois St., Golden, CO 80401, USA, Fax: 303-273-3730.

interactions (i.e. lubrication forces, non-specific adhesion) from cell mechanical properties. These types of interactions can be avoided by using hydrodynamic forces in combination with inertial focusing,[25] which has measurement rates as high as ~2,000 cells/s.[25] While the throughput of this technique is high, the high shear rates (175,000 s^{-1}) and corresponding destructive shear stresses (1,750 dyn/cm^2) in such devices may damage biological samples and can prevent subsequent cell investigation. Such stresses are well above typical physiological values for veins and arteries (of order 1–10 dyn/cm^2).[26] Furthermore, high shear stresses can induce changes in cell mechanical properties making quantification of cell properties difficult. For example, when exposed to shear stresses on the time scale of minutes, RBCs lyse at 1,500 dyn/cm^2,[27] platelets become activated at 80 dyn/cm^2 [28] and leukocytes lyse or experience phenotypic changes at shear stresses above 600 dyn/cm^2.[29,30]

In this manuscript we describe a new cell deformation cytometry technique based on optical alignment compression (OAC) where an extensional flow-field is used with a linear optical trap[31] to force cells to meet or 'collide' at the stagnation point. Rather than using inertial or optical forces to deform cells however, viscous stresses induced by flow around a stationary cell pair are employed to deform cells. To create a cell pair in laminar flow, forced alignment and positional control of incoming cells is necessary. To apply the necessary forces, a linear optical trap,[31] created using an inexpensive laser diode, is used to non-destructively and non-invasively align cells for interaction with optical powers well below intensities capable of stretching[22] or damaging[32,33] cells. Here, the linear optical trap is employed along the direction of flow to position incoming cells for contact at the device center. While the force applied to a single cell at the stagnation point is not sufficient to induce measurable deformation, the hydrodynamic forces acting on a cell pair push cells against one another and are large enough to significantly deform them, allowing for quantification of cell viscoelastic behavior using a simple constitutive model. In these initial studies using this approach we have deformed populations of individual normal, fixed, and a mixed population of 70% normal and 30% fixed RBCs at a rate of ~20 cells/min.

Theory

Figure 1 shows the geometry and salient features of our approach where a diluted whole blood solution is directed in opposing inlet streams toward the center of a cross-junction, creating a stagnation point. The linear optical trap is used to direct cells into the center streamline, forcing them to contact each other at the stagnation point where hydrodynamic drag acting on each cell pushes them together. This creates an effective compressive force that deforms cells during their interaction (Figure 1). We approximate this compressive drag force with Stokes' law, $F = 6\pi\mu Rv$, where μ is the fluid viscosity, R is the average cell radius, and v is the fluid velocity along the long axis of the laser trap.

To convert measured experimental data into cell mechanical properties we use the Kelvin-Voigt (KV) model,[34] a commonly used viscoelastic model to describe RBCs:[35–38]

$$F = kx + \eta \frac{dx}{dt} \quad (1)$$

where F is the applied force (drag force), k the elastic constant (μN/m), η the viscous constant (μN s/m), x the displacement from equilibrium cell shape quantified by the change in equivalent cell diameter, and t the time, starting at initial cell-cell contact. Integrating Eq. 1 with an initial condition of $x(t) = 0$ and assuming a constant applied force yields

$$\frac{x(t)}{F}=\frac{1}{k}\left[1-e^{-kt/\eta}\right] \quad (2)$$

which we use to extract k and η from our experimental data. As it is applied here, our approach assumes that the cells involved in each individual collision are of similar size and experience an equivalent force.

Materials and Methods

In our experiments, an inverted light microscope was used to image the cell-cell interactions in a microfluidic device (Figure 2). In this, two identical dry objectives (40× 0.66 NA, Leica, Wetzlar, Germany) mounted in a caged optics system were used to directly image a 200 × 1 μm^2 5 W 808 nm linear diode laser (China Daheng Group, Inc., Beijing, China) at the device flow stagnation point, creating a linear optical trap (Figure 1). Without the need for scanning or sophisticated and expensive optical phase manipulation, this simple technique was used to create an effective one-dimensional optical trap[31] extending a significant distance from the stagnation point and into the cell flow inlet. The laser power applied at the focal plane ranged from 100–200 mW down the length of the laser, resulting in less than 1 mW/μm on trapped cells, well below powers previously used to manipulate (4–100 mW)[32,33] and stretch (10–40 mW/μm)[22] RBCs. Staining with Trypan blue (Sigma, St. Louis, MO) was used both before and after testing to determine if cell viability was affected as a result of measurement. Images were captured with a CCD camera (SV9M001, Epix, Inc., Buffalo Grove, IL) at 100 frames/s and ~10 ms shutter times.

Blood was obtained from healthy donors according to the Declaration of Helsinki and IRB-approved protocol where, following sterilization with alcohol, a contact-activated lancet (BD, Franklin Lakes, NJ) was used to puncture the skin. 13.5 μl of blood was collected off the finger with a micropipette and transferred to a suspension buffer solution of phosphate buffered saline (PBS) solution (34 mM NaCl, 0.7 mM KCl, 0.4 mM KH_2PO_4, and 1.6 mM Na_2HPO_4), 0.15% bovine serum albumin (BSA) and 1.1% sodium citrate to inhibit coagulation. The final solution osmolarity was 225 mOsm, which induced slight swelling of the cells. To compare multiple populations, we measured the deformation of normal and glutaraldeyde-fixed RBCs. Glutaraldehyde is a non-specific cross-linker of proteins that stiffens the cell without a significant change in shape[39] and was added to a final concentration of 0.01% v/v to the suspensions described above. Mixed cell populations were generated by combining PBS-washed, fixed RBCs with normal RBCs in a volume ratio of 30% fixed to 70% normal cells.

Microfluidic devices with channels 100 μm wide and 10 μm in height were fabricated using standard soft lithography techniques[40] and bonded to glass cover slips following treatment with an oxygen plasma. The device includes a single inlet that bifurcates into two streams, which re-converge to create the device cross junction and stagnation point (Figure 1), a design similar to other microfluidic systems that employ extensional flow.[41,42] Devices were first incubated with blood-free suspension solution for 1 hr prior to experiment. A 3 ml Luer-Lok syringe (BD, Franklin Lakes, NJ) connected with a 30 gauge stainless steel blunt needle (Small Parts, Inc., Logansport, IN) to 0.01″ ID Tygon tubing (Saint-Gobain, Valley Forge, PA) was used as a reservoir and to transfer the RBC suspension (~2×10^5 cells/μl) into the microfluidic device. Velocities of 50–60 μm/s were reached using a pressure head of 10 cm of solution. The stagnation point of the device was then aligned with the laser trap in the optical setup (Figure 1) and videos of cell-cell collisions acquired for image analysis.

Images were analyzed using custom scripts and built-in routines in the MATLAB Image Processing Toolbox (Mathworks, Natick, MA). These scripts are available for download on the Mathworks File Exchange (www.mathworks.com/matlabcentral/fileexchange, File ID: #36816). Each grayscale image was processed with the following steps: (i) threshold using Otsu's method, (ii) edge detection using the Sobel method, (iii) connected components filled, and (iv) small objects (less than 20 μm^2) removed. Due to the anisotropic shape and varying orientation of colliding cells at 225 mOsm, departure from initial cell shape was quantified as a change in equivalent diameter, defined as the diameter of a circle with the same area as the cell. Cell velocities during each collision were measured by tracking the centroid of the incoming cell in flow at approximately one cell diameter from the stagnation point. In the rare event that the centroids were not aligned within 2 μm, corresponding to a 5% measurement error, the measurement was omitted. Nonlinear least squares regression was performed to fit Eq. 2 with the data (MATLAB Curve Fitting Toolbox). A two-sample *t*-test was performed between normal and fixed cell samples to determine differences in *k* and η with the null hypothesis tested at a 5% significance level.

Results

We have shown that by combining an extensional flow field with a linear optical trap in a microfluidic device, we can develop a non-destructive cell deformation cytometer. The non-destructive nature of OAC cytometry was confirmed with Trypan blue staining before and after testing, indicating no loss of RBC viability following measurement by OAC. Figure 3 demonstrates the approach and the progression of events in a representative cell-cell interaction. First, a single cell is held in place at the flow stagnation point by the linear trap (Figure 3a) using low optical powers sufficient to simply hold the cell until the next cell arrives. The same optical trap then aligns an incoming cell as necessary to form a cell-cell pairing at the stagnation point where it is exposed to hydrodynamic flow and associated viscous stresses sufficient for deformation. The trap is then momentarily deactivated to release the cells and, without the trap present, cells are pushed out by fluid flow, leaving the stagnation point open to trap and deform a new cell pair. In this, the extensional flow field not only acts to bring cells together, but also removes cells from the stagnation point after deformation. With a fluid velocity of 50–60 μm/s ($F \approx 3.3$ pN), time from cell contact to full deformation is just under 0.15 s (Figures 3 & 4). At the flow rate of ~0.05 nl/s used in our experiments, ~1 s was required to clear the stagnation point. At the associated cell dilution (~2×10^5 cells/μl), we observed a throughput of ~10 collisions/min or deformation rates of ~20 cells/min.

The dynamics of each cell-cell collision are dominated by different characteristic behaviors upon initial and during later-stage deformation (Figure 4). Initially, cell deformation follows the limit of Eq. 2 at short times where $x(t)/F$ is linear, with a slope of $1/\eta$,

$$\lim_{t\to 0}\frac{x(t)}{F}=\frac{1}{\eta}t; \quad (3)$$

however, as cells reach full compression, deformation approaches $1/k$,

$$\lim_{t\to \infty}\frac{x(t)}{F}=\frac{1}{k}. \quad (4)$$

Figure 4 shows representative raw data for both normal and fixed RBCs, along with lines denoting the nonlinear regression of Eq. 2 used to calculate *k* and η. Both cells are shown for each collision, including trapped and incoming cells.

In our studies, there was a significant difference (two-sample *t*-test, $p < 0.001$) in *k* measured between normal (8.62 ± 3.10 μN/m) and fixed (17.1 ± 7.55 μN/m) RBCs (Figures 5 & 6 and Suppl. Fig. 1). Because the forces applied were the same, fixed cells deform less than normal cells, corresponding to the observed increase in *k*. On the other hand, there was no significant difference in η measured between the normal (1.21 ± 0.69 μN s/m) and fixed (1.15 ± 0.75 μN s/m) RBCs (Figures 5 & 6), suggesting similar viscous behavior with the amount of fixative not changing η to a degree detectable by OAC. Residual plot analysis indicates that there is no systematic error in curve fitting of either sample.

The representative data in Figure 4 also demonstrates that the mechanical constants extracted from OAC are independent of the orientation of RBC under the conditions used in this study. For example, in Figure 3, the incoming cell (top) and trapped cell (bottom) are in different orientations. Both cells have the typical RBC shape in a 225 mOsm solution, slightly swollen and concave on one side. Though the dimple of each cell is oriented in a different direction, no significant difference between the deformations of two normal cells was observed (Figure 4), an orientation independence also observed in measurements of fixed RBCs.

Discussion

In this study we have developed a technique that employs hydrodynamic drag in conjunction with extensional flow to deform cells colliding at the stagnation point, an approach that has the potential to attain high-throughput measurement rates with less risk of cell damage. While individual cell testing techniques such as micropipette aspiration and atomic force microscopy are capable of accurately measuring the properties of single cells, their throughputs are not adequate for collecting population data. On the other hand, high-throughput techniques such as electroporation and inertial focusing provide significantly larger data collection rates, but can damage the tested cells. This new approach is able to non-destructively measure the mechanical properties of cells as well as generate population data. This technique also takes advantage of the geometry of the linear optical trap where we have previously demonstrated that such anisotropic traps can sort[31,43] and stretch[22,44] cells at high power. In OAC, however, hydrodynamic forces, not optical forces, induce cell deformation and the optical trap is used as an alignment tool only. As a result, the optical trap intensity is an order of magnitude lower[22] and does not contribute to cell deformation.

To quantify cell deformation, mechanical properties for each cell were determined using measured deformation with the KV model where properties are separated into elastic and viscous contributions. Standard viscoelastic membrane behavior is shown in the limits of the KV model with the rate of membrane deformation controlled by η (Eq. 3), and the extent of deformation controlled by *k* (Eq. 4).[7] The elasticity of a cell can be divided into three contributions: the shear modulus, the area expansion modulus, and the bending modulus.[13] Since area dilation does not occur during OAC experiments, it can be neglected. The bending modulus in RBCs is much smaller than the elastic modulus,[45] allowing one to equate the calculated elastic constant and the elastic shear modulus. Reported values of elastic shear modulus for RBCs range from 2.5–13.5 μN/m,[20,35,46–48] which is in agreement with our results for *k* (8.62 ± 3.10 μN/m) by OAC. The total membrane viscosity was found by Evans and Hochmuth (1976) to be ~1 μN s/m,[45] which is comparable to our results for η (1.21 ± 0.69 μN s/m) of the normal cell population.

For fixed cells we observed an increase in *k* in agreement with previous findings.[39] Due to fixation with glutaraldehyde, the RBC membrane is stiffened, resulting in less deformation and a higher measured *k*. There was no difference, however, between η in the two cell populations. The viscoelastic nature of the RBC is controlled by the cytoskeleton,[7] while the

viscous contribution of the lipid bilayer and fluid cytoplasm have little effect on the deformation and relaxation response of the cell.[13,35,45,49] Because of the relative contribution of k and η, it is expected that the major difference between the normal and fixed RBC populations will be found in the value of k.

Demonstrating such detectable differences in a mixed population without tags, in Figures 5 and 6 we measure a sample of 30% fixed to 70% normal cells and compare results to those determined independently above. In this case and fitting to two populations (Supp. Fig. 1), we find k = 5.96 ± 3.11 μN/m and 12.3 ± 6.76 μN/m and η = 0.64 ± 0.09 μN s/m and 0.80 ± 1.79 μN s/m with the stiffer population at 41% ± 9.7% of the total. These results are indeed consistent and demonstrate the utility of OAC cytometry as a testing method, able to identify separate cell populations in a mixture without cell tagging.

Using the conditions reported in this study, we measured cell mechanical properties at a rate of ~20 cells/min, a value chosen to determine technique viability and methods. The theoretical throughput of OAC however is limited by the cell relaxation time (τ), the time required for a cell to recover from a deformed state. In this technique, a small force is applied and cells respond by deforming at a rate set by τ. Though much higher forces could be applied, our reversible approach provides access to cell deformation dynamics, allowing measurement of both viscous and elastic properties. Because two cells are deformed at the same time, two measurements are simultaneously recorded, allowing for a maximum throughput of $2/\tau$. For RBCs with τ = 0.1 s,[13,37] a maximum throughput of 20 cells/s is expected. While this technique does not approach the throughputs available with traditional cytometry, it instead offers a nondestructive technique for measuring the individual cell properties of small populations. Cytometry methods trade testing at lower, physiological shear rates for increases in throughput that risk damaging cells with high shear and contact forces, problems that OAC avoids. The ability to test cells in a non-invasive, non-destructive manner allows for further testing on viable cells. Studying deformation in this manner also allows for investigation into shear stress sensitive cells such as leukocytes[29,30] and platelets.[28]

OAC cytometry can be used to measure deformation in non-spherical cell systems as well, as shown here with RBCs. Normal RBCs exhibiting shape anisotropy will readily rotate in an optical trap;[50] however, optical trap intensities were kept low and cells were slightly swollen to minimize rotation and observe the orientation independence of RBC properties. One could, however, readily employ slightly higher intensities that would tightly pre-orient cells for those systems that do not adopt spherical shapes, such as sickled RBCs.

Conclusion

In conclusion, we demonstrate that a linear optical trap and a microfluidic extensional flow device can be combined to create an individual cell mechanical property testing cytometer. The approach has the ability to measure properties in a non-destructive, non-invasive manner and can independently measure cell elastic and viscous response. While throughput can still be significantly improved, techniques that can identify changes in mechanical properties while still preserving cells for subsequent testing and/or growth, will become increasingly useful as more comprehensive microfluidic systems are developed.

Supplementary Material

Refer to Web version on PubMed Central for supplementary material.

Acknowledgments

The authors gratefully acknowledge support from the National Institutes of Health's National Institute of Allergy and Infectious Diseases under grants 1R01 AI079347 and 1R01 AI063366. The authors would also like to thank Benjamin Johnson, Katelyn Hoden, Aditya Kasukurti and Tobias Sawetzki for helpful discussions.

References

1. Suresh S. Acta Mater. 2007; 55:3989–4014.
2. Hoffman BD, Crocker JC. Annu Rev Biomed Eng. 2009; 11:259–288. [PubMed: 19400709]
3. Li QS, Lee GYH, Ong CN, Lim CT. Biochem Biophys Res Commun. 2008; 374:609–613. [PubMed: 18656442]
4. McMillan DE, Utterback NG, La Puma J. Diabetes. 1978; 27:895–901. [PubMed: 689301]
5. Baskurt O, Gelmont D, Meiselman H. Am J Respir Crit Care Med. 1998; 157:421. [PubMed: 9476853]
6. Nash G, Brien EO, Gordon-Smith E, Dormandy J. Blood. 1989; 74:855–861. [PubMed: 2665857]
7. Stuart J, Nash G. Blood Rev. 1990; 4:141–147. [PubMed: 2245249]
8. Bull B, Feo C, Bessis M. Cytometry. 1983; 3:300–304. [PubMed: 6822151]
9. Bessis M, Mohandas N, Feo C. Blood Cells. 1980; 6:315–327. [PubMed: 7397390]
10. Jandl JH, Simmons RL, Castle WB. Blood. 1961; 18:133–148. [PubMed: 13789381]
11. Schmid-Schönbein H, Wells R, Goldstone J. Circ Res. 1969; 25:131–143. [PubMed: 5806159]
12. Evans EA, Waugh R, Melnik L. Biophys J. 1976; 16:585–595. [PubMed: 1276386]
13. Hochmuth RM, Waugh RE. Annu Rev Physiol. 1987; 49:209–219. [PubMed: 3551799]
14. Hochmuth RM. J Biomech. 2000; 33:15–22. [PubMed: 10609514]
15. Weisenhorn AL, Khorsandi M, Kasas S, Gotzos V, Butt HJ. Nanotechnology. 1993; 4:106–113.
16. Radmacher M, Fritz M, Kacher CM, Cleveland JP, Hansma PK. Biophys J. 1996; 70:556–567. [PubMed: 8770233]
17. Lekka M, Laidler P, Gil D, Lekki J, Stachura Z, Hrynkiewicz A. Eur Biophys J. 1999; 28:312–316. [PubMed: 10394623]
18. Wang N, Butler J, Ingber D. Science. 1993; 260:1124. [PubMed: 7684161]
19. Bausch AR, Ziemann F, Boulbitch AA, Jacobson K, Sackmann E. Biophys J. 1998; 75:2038–2049. [PubMed: 9746546]
20. Dao M, Lim C, Suresh S. J Mech Phys Solids. 2003; 51:2259–2280.
21. Guck J, Schinkinger S, Lincoln B, Wottawah F, Ebert S, Romeyke M, Lenz D, Erickson HM, Ananthakrishnan R, Mitchell D. Biophys J. 2005; 88:3689–3698. [PubMed: 15722433]
22. Sraj I, Eggleton CD, Jimenez R, Hoover E, Squier J, Chichester J, Marr DWM. J Biomed Opt. 2010; 15:047010. [PubMed: 20799841]
23. Bao N, Zhan Y, Lu C. Anal Chem. 2008; 80:7714–7719. [PubMed: 18798650]
24. Bow H, Pivkin IV, Diez-Silva M, Goldfless SJ, Dao M, Niles JC, Suresh S, Han J. Lab Chip. 2011; 11:1065. [PubMed: 21293801]
25. Gossett DR, Tse HTK, Lee SA, Ying Y, Lindgren AG, Yang OO, Rao J, Clark AT, Di Carlo D. Proc Natl Acad Sci. 2012; 109:7630–7635. [PubMed: 22547795]
26. Kroll MH, Hellums JD, McIntire LV, Schafer AI, Moake JL. Blood. 1996; 88:1525–1541. [PubMed: 8781407]
27. Leverett LB, Hellums JD, Alfrey CP, Lynch EC. Biophys J. 1972; 12:257–273. [PubMed: 5016112]
28. Shankaran H. Blood. 2002; 101:2637–2645. [PubMed: 12456504]
29. Dewitz TS, Hung TC, Martin RR, McIntire LV. J Lab Clin Med. 1977; 90:728–736. [PubMed: 903701]
30. Dewitz TS, McIntire LV, Martin RR, Sybers HD. Blood Cells. 1979; 5:499–512. [PubMed: 555700]

31. Applegate RW, Squier J, Vestad T, Oakey J, Marr DWM. Opt Express. 2004; 12:4390–4398. [PubMed: 19483988]
32. Ashkin A, Dziedzic J, Yamane T. Nature. 1987; 330:769–771. [PubMed: 3320757]
33. Mohanty SK, Uppal A, Gupta PK. J Biophoton. 2008; 1:522–525.
34. Fung, Y-C. Biomechanics: Mechanical Properties of Living Tissues. 2. Springer; New York: 1993.
35. Hochmuth RM, Worthy PR, Evans EA. Biophys J. 1979; 26:101–114. [PubMed: 262407]
36. Evans E, Mohandas N, Leung A. J Clin Invest. 1984; 73:477–488. [PubMed: 6699172]
37. Mauritz JMA, Tiffert T, Seear R, Lautenschläger F, Esposito A, Lew VL, Guck J, Kaminski CF. J Biomed Opt. 2010; 15:030517. [PubMed: 20615000]
38. Tomaiuolo G, Barra M, Preziosi V, Cassinese A, Rotoli B, Guido S. Lab Chip. 2011; 11:449. [PubMed: 21076756]
39. Heusinkveld RS, Goldstein DA, Weed RI. Blood Cells. 1977; 3:175–182.
40. Duffy D, McDonald J, Schueller O, Whitesides G. Anal Chem. 1998; 70:4974–4984. [PubMed: 21644679]
41. Nève N, Kohles SS, Winn SR, Tretheway DC. Cell Mol Bioeng. 2010; 3:213–228. [PubMed: 20824110]
42. Tanyeri M, Ranka M, Sittipolkul N, Schroeder CM. Lab Chip. 2011; 11:1786. [PubMed: 21479293]
43. Applegate RW, Squier J, Vestad T, Oakey J, Marr DWM. Appl Phys Lett. 2008; 92:013904.
44. Sraj I, Marr DWM, Eggleton CD. Biomed Opt Express. 2010; 1:482–488. [PubMed: 21258483]
45. Evans EA, Hochmuth RM. Biophys J. 1976; 16:1–11. [PubMed: 1244886]
46. Guck J, Ananthakrishnan R, Mahmood H, Moon TJ, Cunningham C, Käs J. Biophys J. 2001; 81:767–784. [PubMed: 11463624]
47. Waugh R, Evans EA. Microvasc Res. 1976; 12:291–304. [PubMed: 1004241]
48. Henon S, Lenormand G, Richert A, Gallet F. Biophys J. 1999; 76:1145–1151. [PubMed: 9916046]
49. Forsyth AM, Wan J, Ristenpart WD, Stone HA. Microvasc Res. 2010; 80:37–43. [PubMed: 20303993]
50. Bambardekar K, Dharmadhikari JA, Dharmadhikari AK, Yamada T, Kato T, Kono H, Fujimura Y, Sharma S, Mathur D. J Biomed Opt. 2010; 15:041504. [PubMed: 20799782]

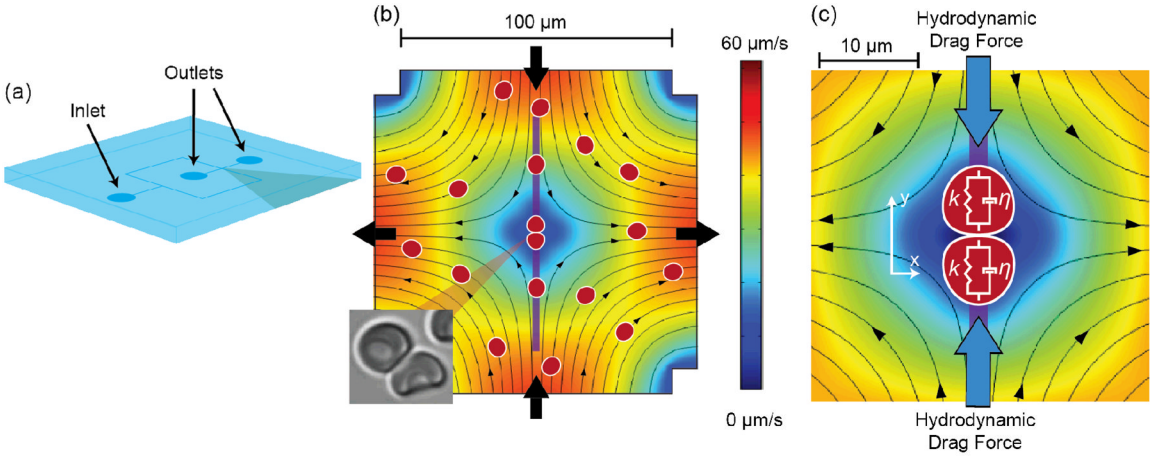

Figure 1.

Extensional flow geometry. (a) Device schematic where a single bifurcated inlet comes together to create a cross-junction and flow stagnation point. (b) Detailed view of the cross-junction, with cells entering and exiting the stagnation point. The arrows indicate streamlines, while the optical trap (purple) aligns cells for contact at the stagnation point. (c) Kelvin-Voigt elements in a collision with hydrodynamic drag force compressing them together.

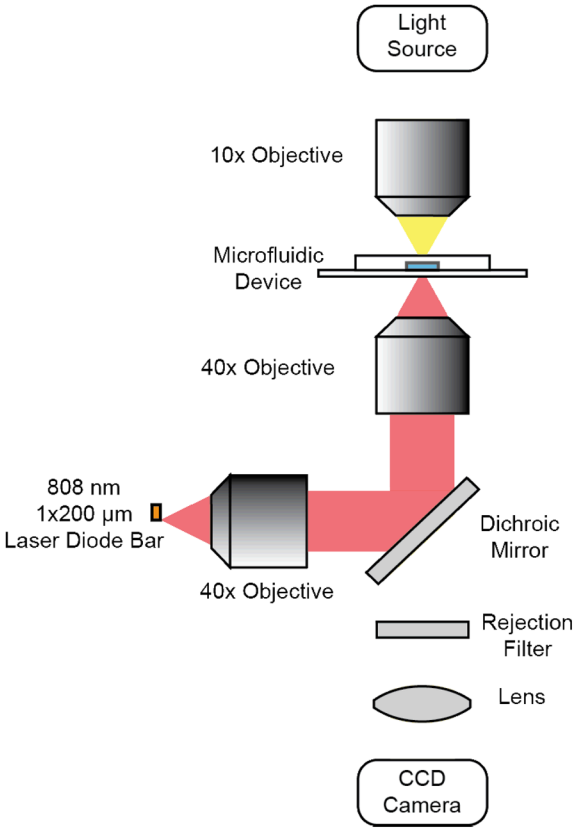

Figure 2.
Optical setup. A laser diode bar is collimated with a 40x objective and focused at the imaging plane using an identical objective. The 10x objective is used to condense light for imaging on the CCD camera below the focal plane. An additional lens (f = 250 mm) magnifies the image on the CCD while a rejection filter blocks laser light to the camera.

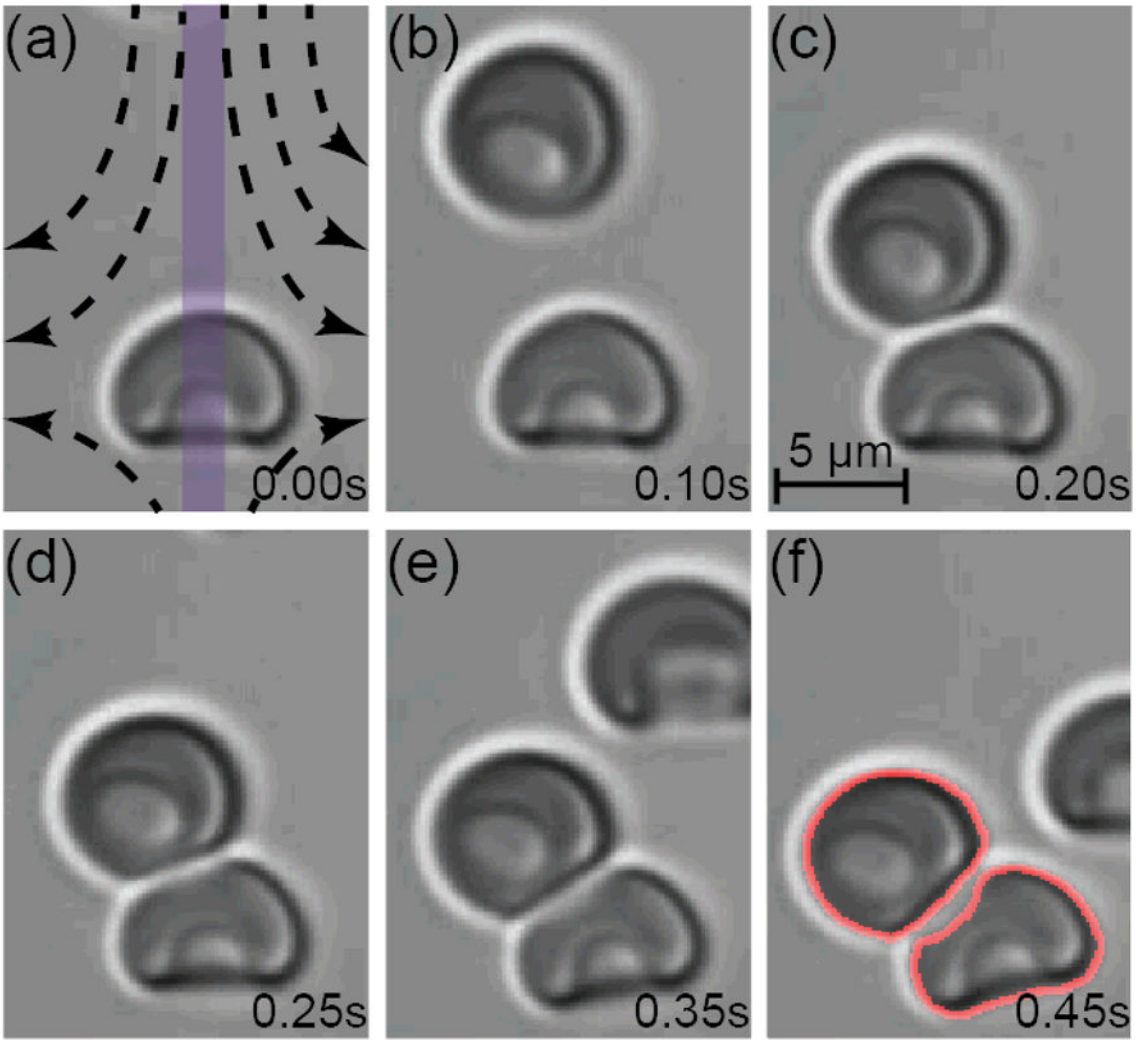

Figure 3.
Typical RBC collision. Streamlines are shown in (a) along with the linear optical trap, illustrated in purple. The result of image processing is shown as the outline in (f). See also Suppl. Video 1.

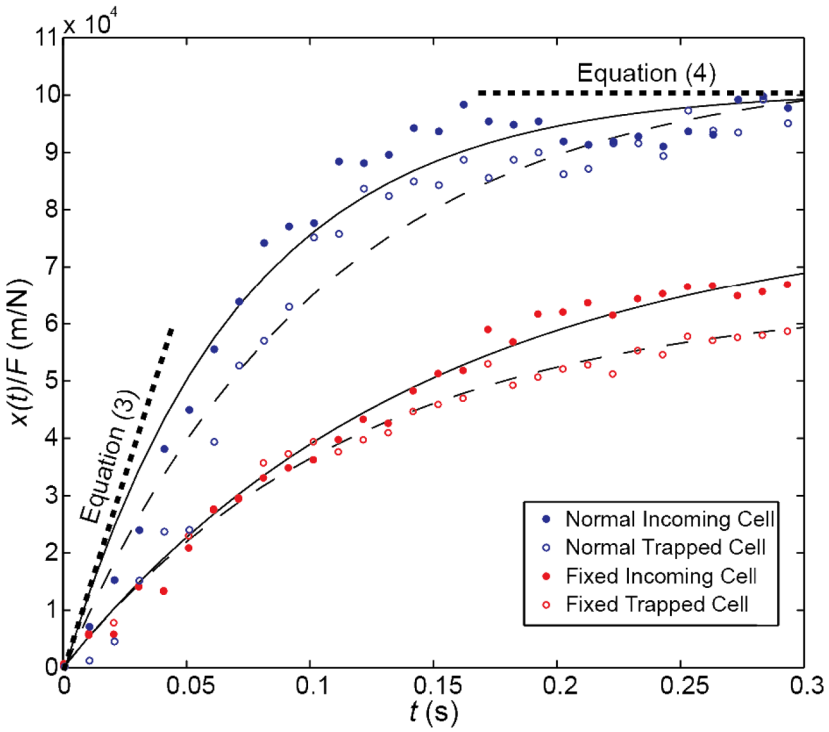

Figure 4.

Image processing data with fit. The normal cell data corresponds to the collision event depicted in Figure 3 from initial contact to full deformation. Data fits for the trapped (dashed thin line) and incoming (solid thin line) are also shown overlaid on the data. For reference, the limits described by Eq. (3) and (4) are also shown as thick dashed lines. Data fitting using the MATLAB Curve Fitting Toolbox to the model yielded R^2 values from 0.7 to 0.9.

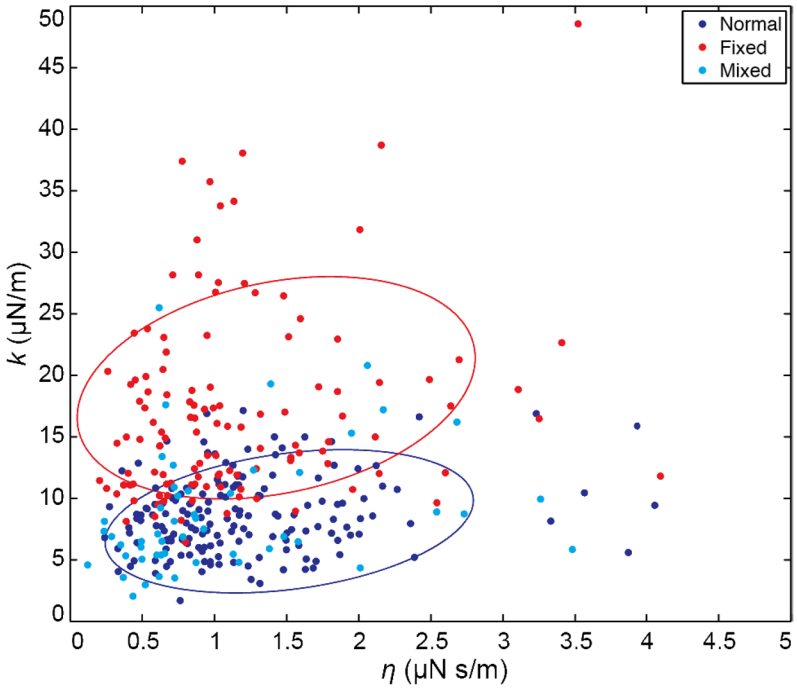

Figure 5.
Population data for 165 normal (blue), 121 fixed (red) cells and 52 cells from a mixed cell sample (cyan). Data shown is for all measured cells, trapped and incoming.

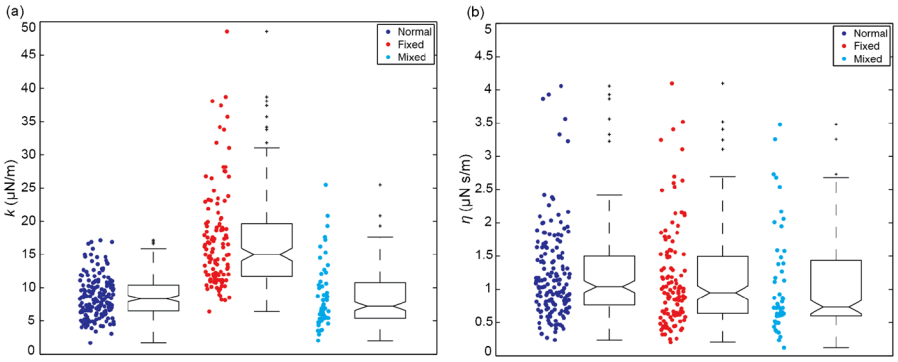

Figure 6.

Population data: (a) Elastic and (b) viscous constants for normal, fixed, and mixed cell populations. Standard box plots show the middle 50% of data for the normal and fixed samples, crosses designate statistical outliers. A two-sample *t*-test demonstrated a statistical difference between *k* for normal and fixed cells ($p<0.001$). Using the same test, no statistical difference was found between normal and fixed cell populations for η.